RESONANCE COMPENSATION STUDIES AT THE FNAL RECYCLER RING

By

Cristhian Gonzalez-Ortiz

A DISSERTATION

Submitted to
Michigan State University
in partial fulfillment of the requirements
for the degree of

Physics—Doctor of Philosophy

2024

ABSTRACT

ACKNOWLEDGEMENTS

Your acknowledgements here.

TABLE OF CONTENTS

LIST OF ABBREVIATIONS

MSU Michigan State University

FNAL Fermilab National Accelerator Laboratory

RR Recycler Ring

MI Main Injector

RDTs Resonance Driving Terms

NuMI Neutrinos at the Main Injector

PSB CERN Proton Synchrotron Booster

CHAPTER 1

INTRODUCTION

Particle accelerators are the workhorses for modern scientific discoveries. Experimental nuclear and particle physics research benefit greatly from the progress of accelerator physics and technology. Accelerator physics is a rich field of applied physics living on the intersection of electromagnetism, solid-state and atomic physics, nonlinear mechanics, plasma physics, quantum mechanics, just to name a few [1]. Furthermore, the design and operation of modern accelerator projects require costly enterprises of scientists, engineers, operators, and politicians coming together under one single metaphorical roof.

The scientific principle of particle accelerators involves the acceleration, steering and/or storage of charged particles through electromagnetic manipulations. These manipulations occur through a plethora of devices and components that can control electromagnetic fields, e.g., magnets, electrical cavities. The group of particles that is subject to this electromagnetic steering is referred to as the beam. The field of beam dynamics studies the interaction between the beam and the steering devices, as well as the Coulomb interactions between the beam itself—this is usually known as space charge physics. An additional distinction can be made when these steering devices are configured in a circular or linear fashion. This gives rise to the distinction between circular accelerators and linear accelerators (Linacs).

Furthermore, particle accelerators can be categorized by the type of elementary particles that compose the beam and how close to the speed of light they are traveling. The first category refers to the distinction between hadrons and leptons—particles that interact or do not interact through the strong force, respectively [2]. For example, protons and heavy ions are considered hadrons, while electrons and muons are considered leptons. The second category can be summarized if particles in the machine travel at a high or low energy. An example of a low-energy hadron machine is the heavy ion Linac at FRIB (Facility for Rare Isotope Beams). An example of a high-energy lepton machine was the Stanford Linear Accelerator located at SLAC National Accelerator Laboratory. The two most famous high-energy hadron machines in history are the Tevatron, which operated

at Fermilab, and the LHC (Large Hadron Collider), operating at CERN. Furthermore, there are accelerator projects that encompass several categories such as the future EIC (Electron-Ion Collider) at Brookhaven National Laboratory, which will use an electron ring—a lepton machine—and a heavy-ion circular accelerator—a hadron machine—to probe new physics. This is just to name a few. There's a plethora of accelerator projects around the world that are either operational, under commissioning or being designed.

The following thesis will explore the beam dynamics of a circular machine used to store high-energy protons such as Fermilab's Recycler Ring.

1.1 Circular Accelerators and Storage Rings

As will become more apparent on Ch. 2, a particle accelerator can be thought of as a composition of accelerator-themed LEGO® bricks [3]. Each elemental LEGO® brick can be thought of as an accelerator component performing some mapping on the charged particles entering it. As it turns out, these LEGO® bricks can be assembled together in a circular fashion to give rise to circular accelerators. For the case where particles are not accelerated on these structures, a storage ring arises.

Circular accelerators are special due to the fact that particles have to pass thousands or even millions of turns through the same accelerator elements. This gives birth to very interesting and complex dynamics inside these machines.

1.2 Fermilab

The Fermi National Accelerator Laboratory (FNAL), better known as Fermilab, has a long and rich history of designing, building and operating high-energy particle accelerators. Ever since the founding director of Fermilab, Robert R. Wilson, envisioned the 400 GeV Main Ring back in 1967, Fermilab has been at the forefront of accelerator physics. [4],[5]

As of 2024, the Fermilab Accelerator Complex is composed of an H^- source that connects to a linear accelerator. This linear accelerator feeds to the Booster where protons are achieved and accelerated to an energy of 8 GeV. . A more detailed study of the Fermilab Accelerator Complex

1.3 Outline

The following thesis will explore the compensation of third-order resonances in the Fermilab Recycler Ring. This first chapter introduces the motivation behind this thesis work. The second chapter summarizes single particle dynamics with the help of exponential Lie operators and moves forward to introduce a relevant concept of collective beam dynamics: the space charge tune shift. This theoretical overview gives segue into the third chapter of this thesis, where the Recycler Ring is introduced and described in detail. Motivation for the compensation of third order resonances is given in this chapter under the framework of current and future operation of the RR. With the basic physics concepts and the description of the machine put in place, the fourth chapter describes in full detail the scheme and experiments developed in order to compensate third order resonances at low intensities. Before moving to explore the Recycler Ring at high intensities, chapter five provides an interlude in order to show a series of experiments done at the CERN PS Booster. These experiments explore the use of advanced optimization algorithms in the aid of compensating multiple resonance lines simultaneously. Coming back to Fermilab, chapter six showcases the studies and experiments done at high intensities in the RR in order to understand the interplay between the compensation of resonance lines and space charge effects. Finally, chapter seven brings down the curtain by providing some general conclusions and future work stemming from this thesis.

CHAPTER 2

BEAM DYNAMICS IN RINGS

2.1 Introductory Accelerator Physics

The basic building blocks of a particle accelerator are the elements that steer and focus the beam in the transverse direction. While there are a handful of electromagnetic devices that can do this, the most prominent ones are pure dipole magnets for steering and pure quadrupole magnets for focusing. Nevertheless, some machines such as the Recycler Ring have combined function magnets which can have both types of magnets—and even higher order magnets—embedded in one, in order to steer and focus the particles. The previous information assumes that every magnet can be expanded and described as a decomposition of magnetic multipoles, where dipole and quadrupole components are the lowest order terms of the expansion. Therefore, using the Beth representation [1], the multipole expansion for an arbitrary mutipole magnet reads:

$$B_y(x,y) + iB_x(x,y) = B_0 \sum n = 0^{\infty} \tag{2.1}$$

2.2 Lie Maps in Accelerator Physics

The most basic element of a particle accelerator can be thought of as a LEGO® brick acting as a black box transformation for a single particle. This black box takes some single charged particle with initial transverse coordinates $\left(x_0, x_0', y_0, y_0'\right)$, as defined in a Frenet-Serret coordinate system, and maps them to some final coordinates $\left(x_f, x_f', y_f, y_f'\right)$. For simplicity, any longitudinal effect will not be taken into account for this analysis, but can be easily incorporated. By gathering the initial coordinates into a vector, i.e. $\vec{X}_0 = \left(x_0, x_0', y_0, y_0'\right)$, and doing the same for the final coordinates, i.e., $\vec{X}_f = \left(x_f, x_f', y_f, y_f'\right)$, one can define the mapping $\mathcal{M}$ that relates both vectors, such that:

$$\vec{X}_f = \mathcal{M}\vec{X}_0. \tag{2.2}$$

For a charged particle inside some accelerator element that can be described using Hamiltonian dynamics, the mapping $\mathcal{M}$ can be understood in terms of Poisson brackets and exponential Lie operators [3, 6–9].

Let $\vec{X} = (q_1, p_1, \ldots, q_n, p_n)$ be a 2n dimensional vector, made from n pairs of canonical coordinates (q_i, p_i) that make up the $2n$ dimensional phase space. And let two arbitrary functions $f\left(\vec{X}; s\right)$ and $g\left(\vec{X}; s\right)$ be functions of $\vec{X}$ and s, where s plays the role of the independent "time" coordinate. The Poisson brackets $[\bullet, \bullet]$ can be defined as:

$$[f, g] = \sum_{i=1}^{n} \frac{\partial f}{\partial q_i}\frac{\partial g}{\partial p_i} - \frac{\partial f}{\partial p_i}\frac{\partial g}{\partial q_i}. \tag{2.3}$$

Using this definition, one can explicitly write out the Poisson bracket definition for a 4 dimensional phase space described by state vector $\vec{X} = (x, x', y, y')$. This reads:

$$[f, g] = \frac{\partial f}{\partial x}\frac{\partial g}{\partial x'} - \frac{\partial f}{\partial x'}\frac{\partial g}{\partial x} + \frac{\partial f}{\partial y}\frac{\partial g}{\partial y'} - \frac{\partial f}{\partial y'}\frac{\partial g}{\partial y}. \tag{2.4}$$

The Lie operator $: f :$ acts on some function g and is the adjoint operator of the Poisson bracket operator. Its definition reads:

$$: f : g = [f, g]\,. \tag{2.5}$$

This specific $: \bullet :$ notation allows for a compact notation in order to define the exponential Lie operator. The exponential Lie operator of an arbitrary function f is defined as

$$e^{:f:}\bullet = \sum_{k=0}^{\infty} \frac{1}{k!} (: f :)^k \bullet\,. \tag{2.6}$$

For a Hamiltonian system, the mapping of coordinates from $\vec{X}_0$ to $\vec{X}_f$ follows the expression:

$$\vec{X}_f = e^{-\ell:H:}\vec{X}\Big|_{\vec{X}=\vec{X}_0}, \tag{2.7}$$

which is known as a Lie Map [7]. In this case, ℓ corresponds to the integration length of the independent coordinate. For example, for a particle traversing a magnet which has length L, the integration length is $\ell = L$. When looking at the one-turn map, the integration length corresponds to the circumference C of the accelerator over an effective Hamiltonian H_{eff}. Furthermore, if working with action-angle variables, the integration length ℓ would just be the phase advance μ.

2.3 One-turn Map and Normal Form

Such as LEGO® bricks can be put together to create complex structures, accelerator elements can be assembled together to create complex cycloidal structures such as circular accelerators. In such structures, particles will experience the same one-turn mapping over thousands or even millions of turns. The one-turn map $\mathcal{M}_1$ of a circular accelerator is the composition ($\circ$) of mappings from every LEGO® element in the ring. Choosing an arbitrary initial point at $s = 0$ and going around the ring, the one-turn map describes the transformation of coordinates after one turn, i.e., $\vec{X}_{N=1} = \mathcal{M}_1 \vec{X}_0$. This map composition reads:

$$\mathcal{M}_1 = M_{N+1} \circ e^{:h_N:} \circ \cdots \circ e^{:h_2:} \circ M_2 \circ e^{:h_1:} \circ M_1 = M_{N+1} e^{:h_N:} \ldots e^{:h_2:} M_2 e^{:h_1:} M_1, \tag{2.8}$$

where M_i is the matrix representation of a linear mapping, that does not couple $x - y$ plane, e.g., drift space mapping, quadrupole mapping. On the other hand, the map $e^{:h_i:}$ represents any linear or non-linear mapping that can be found around the machine and can be considered a perturbation to the ideal lattice including coupling elements, e.g., skew quadrupoles, higher order multipole elements. Figure 2.1 illustrates the procedure to build the one-turn map for a circular accelerator.

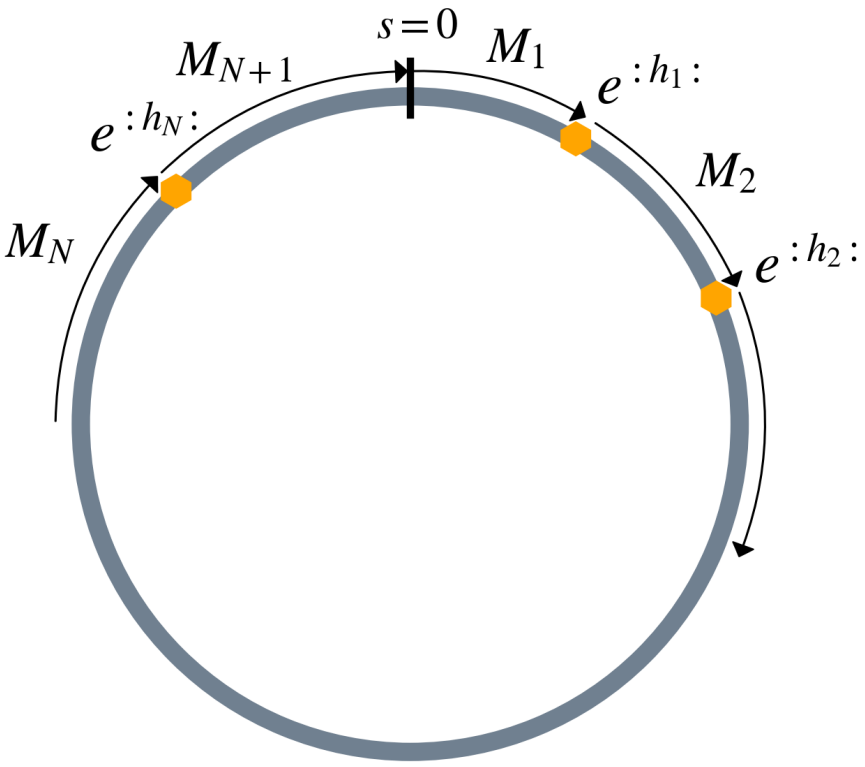

Figure 2.1 Diagram of an arbitrary circular accelerator in order to illustrate the one-turn map.

Through the use of the Baker-Campbell-Hausdorff formula [10], Eq. 2.8 can be collapsed to the expression

$$\mathcal{M}_1 = e^{-C:H_{eff}:}, \tag{2.9}$$

where C is the circumference of the ring and H_{eff} is the effective Hamiltonian of the machine over one turn. As mentioned earlier, for most cases, it is of interest to look at the perturbations to the linear uncoupled dynamics of the design lattice. With this in mind, Eq. 2.9 can be rewritten as:

$$\mathcal{M}_1 = e^{:h:}R, \tag{2.10}$$

where R is a rotation matrix encoding the linear uncoupled dynamics of the ideal lattice. On the other hand, the term $e^{:h:}$ encodes the perturbations to this ideal situation. It is worth pointing out that for the case $h = 0$, the traditional Courant-Snyder variables are recovered.

The Courant-Snyder variables $(\hat{x},\hat{p}_x,\hat{y},\hat{p}_y)$ or normalized phase space coordinates can be written for a linear uncoupled case as:

$$\hat{u} = \sqrt{2J_u}\cos\left(\phi_u + \phi_{u_0}\right); \tag{2.11}$$

$$\hat{p}_u = -\sqrt{2J_u}\sin\left(\phi_u + \phi_{u_0}\right), \tag{2.12}$$

where u can stand either for the x or y coordinate, J_u and ϕ_u correspond to the action-angle variables and ϕ_{u_0} corresponds to the initial phase. For the case where perturbations exist, i.e., $h \neq 0$, the action J_u is not constant anymore and will be a function of ϕ_u.

The Normal Form formalism is introduced at this point in order to find action-angle coordinates I_u and ψ_u, such that the motion just depends on ψ_u at a constant I_u, with some initial phase ψ_{u_0}. These are known as non-linear action-angle variables. The variables I_u and ψ_u are calculated from the transformation $e^{-:F:}$ acting on J_u and ϕ_u. The whole point is to find these variables that allow for the Hamiltonian to be only amplitude dependent. These Normal Form gymnastics can be summarized by the following commutative diagram:

$$\begin{array}{ccc}
\begin{pmatrix} J_x, \phi_x \\ J_y, \phi_y \end{pmatrix}_0 & \xrightarrow{\;e^{:h(J_u,\phi_u):}R\;} & \begin{pmatrix} J_x, \phi_x \\ J_y, \phi_y \end{pmatrix}_f \\
\Big\downarrow{\scriptstyle e^{-:F:}} & & \Big\downarrow{\scriptstyle e^{-:F:}} \\
\begin{pmatrix} I_x, \psi_x \\ I_y, \psi_y \end{pmatrix}_0 & \xrightarrow[\;e^{:H(I_u):}\;]{} & \begin{pmatrix} I_x, \psi_x \\ I_y, \psi_y \end{pmatrix}_f .
\end{array} \tag{2.13}$$

Without loss of generality, the generating function F can be written as a Fourier expansion over the objective space $(I_x, \psi_x, I_y, \psi_y)$ such that:

$$F = \sum_{jklm} f_{jklm} \left(2I_x\right)^{\frac{j+k}{2}} \left(2I_y\right)^{\frac{l+m}{2}} e^{i\left[(j-k)(\psi_x+\psi_{x0})+(l-m)\left(\psi_y+\psi_{y0}\right)\right]}. \tag{2.14}$$

In a similar fashion, the argument of the Lie operator $e^{:h:}$ from Eq. 2.10 can be expanded as:

$$h = \sum_{jklm} h_{jklm} \left(2J_x\right)^{\frac{j+k}{2}} \left(2J_y\right)^{\frac{l+m}{2}} e^{i\left[(j-k)(\phi_x+\phi_{x0})+(l-m)\left(\phi_y+\phi_{y0}\right)\right]}. \tag{2.15}$$

For Eqs. 2.14 and 2.15, the integer indices j, k, l, m run from 0 to infinity, and correspond to the four degrees of freedom for transverse phase space.

The terms f_{jklm} are known as generating function coefficients. The terms h_{jklm} are known as Hamiltonian coefficients or resonance driving terms (RDTs). Section 2.5 will take a closer look into how RDTs can be used to characterize the non-linear dynamics of accelerators. The generating function coefficients f_{jklm} can be related to the Hamiltonian resonance driving terms h_{jklm} through the following relation [8, 11]:

$$f_{jklm} = \frac{h_{jklm}}{1 - e^{2\pi i\left[(j-k)Q_x + (l-m)Q_y\right]}}, \tag{2.16}$$

where Q_x and Q_y represent the transverse uncoupled and unperturbed tunes of the accelerator. The transverse tunes of a circular accelerator are defined as the phase advances in each plane over one turn, in units of 2π, i.e., $Q_u = \phi_u(s = C)/2\pi$.

In general, the terms h_{jklm} are defined by the order in which they enter the one-turn normal form Hamiltonian [11]. The general expression to define RDTs reads:

$$h_{jklm} = \Xi_{jklm} \sum_i L_i \beta_{xi}^{\frac{j+k}{2}} \beta_{yi}^{\frac{l+m}{2}} V_{ni} e^{i\left[(j-k)\phi_{xi} + (l-m)\phi_{yi}\right]}, \tag{2.17}$$

where Ξ_{jklm} is just a constant defined as:

$$\Xi_{jklm} = -\frac{q}{p_0}\frac{1}{2^n}\frac{1}{n}\binom{n}{l+m}\binom{j+k}{j}\binom{l+m}{l}. \tag{2.18}$$

For Eqs. 2.17 and 2.18, $n = j + k + l + m$ represents the order of the resonance. The sum over i is done over all multipoles of order n and length L_i that either have a normal component $V_{ni} = B_{ni}$ if $l + m$ is even, or a skew component $V_{ni} = A_{ni}$ if $l + m$ is odd. The symbols for β_{xi}, β_{yi}, ϕ_{xi} and ϕ_{yi} represent the unperturbed beta functions and phase advances in each plane, respectively.

2.4 Resonances in Circular Accelerators

Equation 2.16 diverges for when the denominator goes to zero. Specifically, this happens when the following condition is met:

$$(j - k)\, Q_x + (l - m)\, Q_y = p, \tag{2.19}$$

where p can be any integer. Equation 2.19 defines resonance lines in tune space of order $n = j + k + l + m$. If the accelerator is tuned to operate on top of these resonances, the perturbations will add up coherently turn to turn and kick the resonant particles out of their original trajectory. In general, operating close or on top of a resonance line is harmful as particles will be lost. This is specially true for lower order resonances, i.e., for $n < 4$. In general, the higher order of a resonance, the weaker it is [12]. This thesis work focuses on third order resonances, i.e., $n = 3$, and how to mitigate their deleterious effect.

Figure 2.2 shows the tune diagram with resonance lines, as defined by Eq. 2.19, drawn up to fifth order. The integer part of both tunes are chosen to include the actual area of operation of the Recycler Ring. Nevertheless, the fractional part of the tune carries the significant information for resonance diagrams. The operation and tune diagram for the Recycler Ring are described in more detail in Ch. 3. Normally, the operation point of a circular accelerator is chosen to be clear of any resonance line and far away as possible from integer ($n = 1$) and half integer ($n = 2$) resonances. Nevertheless, in reality there are two concepts that complicate things. The first one relates to the fact that resonance lines are not infinitely thin and have some stop band width. The second one, concerns the fact that at high intensities particles will not have localized tunes, but rather a distribution of tunes with some tune spread, i.e., a tune footprint. Section 2.6 takes a closer look at this effect known as space charge tune shift. Ultimately, choosing the operation point on Fig. 2.2 is a matter of localizing a resonance-free region where the intensity-dependent tune footprint can be placed.

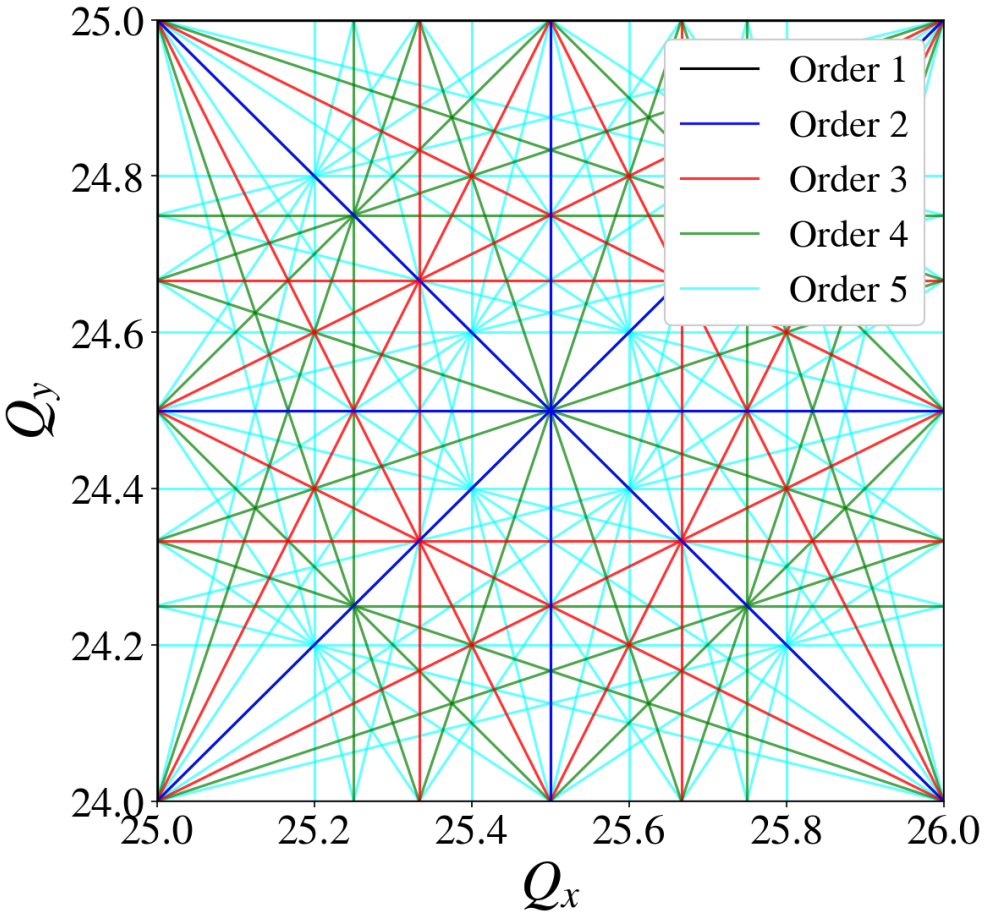

Figure 2.2 Tune diagram with resonance lines up to fifth order, enclosing the operation point of the Recycler Ring.

It is worth stopping here and asking what is the driving force behind each of these resonance lines. Classic accelerator references such as Refs. [1, 6, 12] will derive Eq. 2.19 by perturbing Hill's equation with different magnetic multipole orders. A closer look into each perturbation term reveals that half integer resonances are caused by quadrupole terms, third order resonances by sextupole-like terms, fourth order resonances by octupole terms, and so on and so forth. Nevertheless, the story complicates when one takes into account that pure multipole magnets can feed down to higher order terms, e.g., a tilted quadrupole feeds down to sextupole-like terms.

Figure 2.3 zooms into the region of interest for the Recycler Ring operation in the tune diagram, as shown in Fig. 2.2. As mentioned before, the operation point of an accelerator in the tune diagram is not a singular point but rather a footprint. While the lattice can be tuned to a specific nominal

point, particles will interact with other particles through the Coulomb force. Consequently, each particle will feel a different tune shift depending on their position within the bunch of particles. This is called the incoherent space charge tune shift, and it will be the largest for particles in the core of the bunch, i.e., the beam core. At low particle intensities, such as the one used to produce Fig. 2.3, the tune spread of the particles in the bunch is small enough to approximate the physics to single-particle dynamics. For beams with low particle intensities and a small tune spread, such as the one depicted in Fig. 2.3, operating clear from any low order resonance lines is not generally a problem. Nevertheless, at high intensities the situation changes.

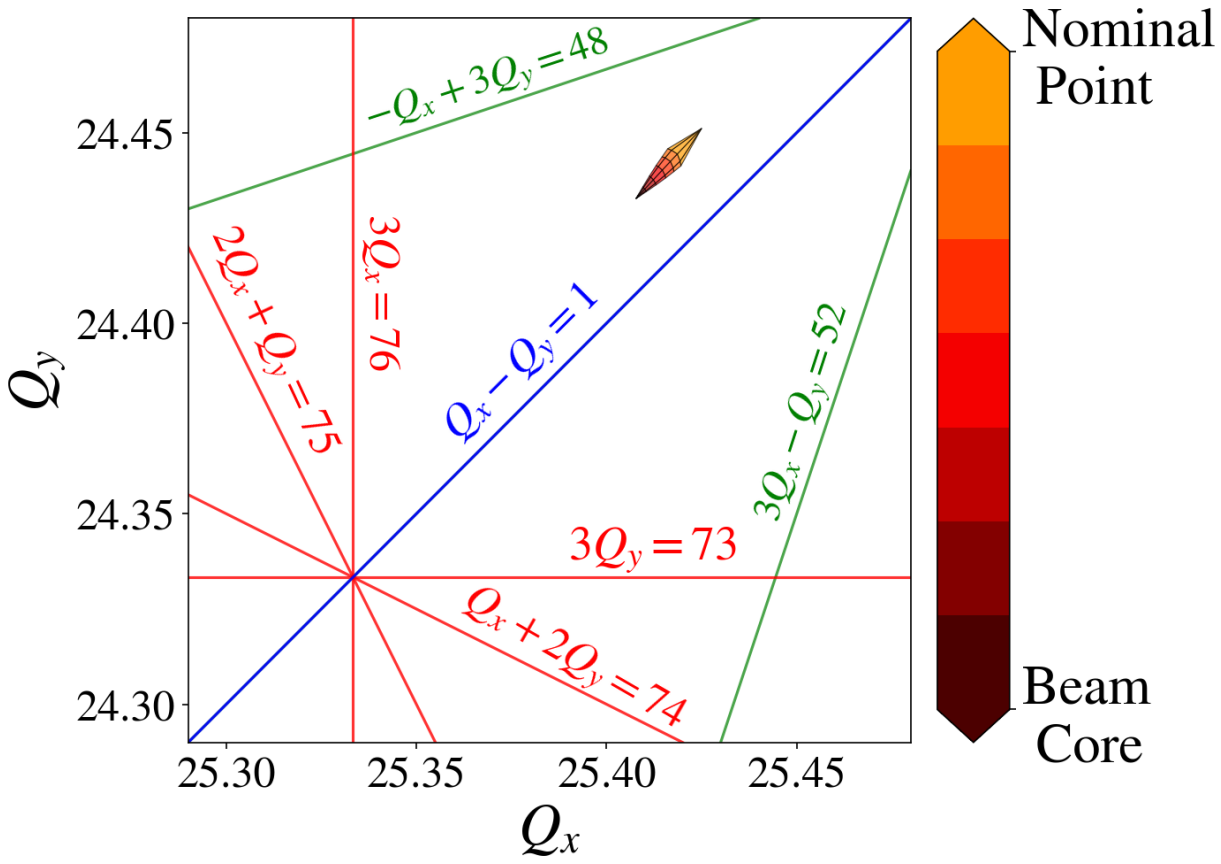

Figure 2.3 Approximate operational tune footprint at low intensities, i.e., 1e10 particles per bunch.

Figure 2.3 plots all resonance lines up to fourth order in this region of interest. The half integer line $Q_x - Q_y = 1$, also known as a difference coupling resonance, is usually driven by solenoidal and skew-quadrupole fields in the lattice. The third order lines $3Q_x = 76$ and $Q_x + 2Q_y = 74$ are

driven by sextupole-like fields. The other third order lines $3Q_y = 73$ and $2Q_x + Q_y = 75$ are driven by skew sextupole terms in the lattice. And finally, the fourth order lines $-Q_x + 3Q_y = 48$ and $3Q_x - Q_y = 52$ are driven by octupole terms in the lattice and Coulomb (space charge) forces from the bunch itself. This is assuming a rectangular multipole expansion notation of the magnetic field, such as the one presented in Ref. [1].

2.5 Resonance Driving Terms

The RDTs h_{jklm} are related to the strength of the resonance $(j-k)\,Q_x + (l-m)\,Q_y$. Therefore, controlling and measuring these RDTs is of special interest to accelerator physics. The following section explains how to get to a useful expression that can be used in order to measure the h_{jklm} terms through Fourier expansions.

The whole point of introducing the Normal Form coordinates (I_u, ψ_u) through the transformation $e^{-:F:}$ as defined in Eq. 2.14 is to transfer complicated non-linear dynamics to simple dynamics that lie on a circle where the action is conserved I_u and $\dot{\psi_u}$ is constant. When this happens, a set of canonical coordinates $\vec{\zeta} = \left(\zeta_x^+, \zeta_x^-, \zeta_y^+, \zeta_y^-\right)$ can be defined as:

$$\zeta_u^{\pm} = \sqrt{2I_u} e^{\mp i\left(\psi_u + \psi_{u_0}\right)}, \tag{2.20}$$

always keeping in mind that I_u is a constant of motion and ψ_{u_0} is a constant initial phase set by the initial conditions. It can be shown that the Poisson brackets for a pair of these quantities are:

$$\left[\zeta_u^+, \zeta_u^-\right]_{\psi_u, J_u} = \frac{\partial \zeta_u^+}{\partial \psi_u}\frac{\partial \zeta_u^-}{\partial J_u} - \frac{\partial \zeta_u^+}{\partial J_u}\frac{\partial \zeta_u^-}{\partial \psi_u} = -2i, \tag{2.21}$$

for the same plane u and using a reduced form of Eq. 2.4. In this notation, the subindices from $[\bullet, \bullet]_{\psi_u, J_u}$ refer to the variables to be used in order to calculate the Poisson brackets. Using Eq. 2.21, the following useful property can be derived:

$$\left[\zeta_x^{+j}\zeta_x^{-k}\zeta_y^{+l}\zeta_y^{-m}, \zeta_x^-\right]_{\psi_x, J_x} = \left(\zeta_y^{+l}\zeta_y^{-m}\right)\left[\zeta_x^{+j}\zeta_x^{-k}, \zeta_x^-\right]_{\psi_x, J_x} = -2ij\zeta_x^{+j-1}\zeta_x^{-k}\zeta_y^{+l}\zeta_y^{-m}, \tag{2.22}$$

where the last step can be achieved using Leibnitz rule for Poisson brackets, i.e., $[fg, h] = [f, h]g + f[g, h]$.

On the other hand, going back to the Courant-Snyder phase space, a set of coordinates known as a resonance basis $\vec{h} = \left(h_x^+, h_x^-, h_y^+, h_y^-\right)$ can be defined. In a similar fashion to Eq. 2.20, the resonance basis reads:

$$h_u^{\pm} = \hat{u} \pm \hat{p_u} = \sqrt{2J_u} e^{\mp i\left(\phi_u + \phi_{u_0}\right)}, \tag{2.23}$$

always keeping in mind that in the Courant-Snyder phase space, the action J_u is a function of the phase ϕ_u, i.e., $J_u = J_u(\phi_u)$ and is not constant. The initial phase ϕ_{u_0} is again a constant set by the initial conditions.

The basis grouped in $\vec{h}$ and the one grouped in $\vec{\zeta}$ are related by the transformation:

$$\vec{h} = e^{:F\left(\vec{\zeta}\right):} \vec{\zeta}, \tag{2.24}$$

where $F(\vec{\zeta})$ is the generating function written in terms of the basis $\vec{\zeta}$. The inverse transformation to Eq. 2.24 reads:

$$\vec{\zeta} = e^{-:F\left(\vec{\zeta}\right):} \vec{h}. \tag{2.25}$$

Writing out the generating function $F(\vec{\zeta})$ in a general polynomial form, this functions reads:

$$F\left(\vec{\zeta}\right) = \sum_{jklm} f_{jklm} \zeta_x^{+j} \zeta_x^{-k} \zeta_y^{+l} \zeta_y^{-m}. \tag{2.26}$$

By inserting the definitions in Eq. 2.20 into Eq. 2.26, the proposed definition in Eq. 2.14 can be recovered.

Expanding Eq. 2.24 by using the exponential Lie operator definition from Eq. 2.6 reads:

$$\vec{h} = \vec{\zeta} + \left[F\left(\vec{\zeta}\right), \vec{\zeta}\right] + \frac{1}{2}\left[F\left[F, \vec{\zeta}\right]\right] + \ldots, \tag{2.27}$$

where this expression was truncated to second order in the Poisson brackets. By taking only the first two terms of the expansion, and introducing the expression from Eq. 2.26, one can find an approximated expression for h_x^- which reads:

$$h_x^- \approx \zeta_x^- + \left[F\left(\vec{\zeta}\right), \zeta_x^-\right] = \zeta_x^- + \sum_{jklm} f_{jklm}\left[\zeta_x^{+j} \zeta_x^{-k} \zeta_y^{+l} \zeta_y^{-m}, \zeta_x^-\right], \tag{2.28}$$

At this point is where the usefulness of Eq. 2.22 comes into play. Introducing the explicit result from Eq. 2.22 into Eq. 2.28 yields the following expression:

$$h_x^- \approx \zeta_x^- - 2i \sum_{jklm} j f_{jklm} \zeta_x^{+j-1} \zeta_x^{-k} \zeta_y^{+l} \zeta_y^{-m}. \tag{2.29}$$

Manipulating this expression further, the definition for ζ_u as described in Eq. 2.20 can be introduced into Eq. 2.29. This yields:

$$\begin{aligned} h_x^-(N) = &\sqrt{2I_x} e^{i\left(\psi_x + \psi_{x_0}\right)} \\ &- 2i \sum_{jklm} j f_{jklm} \left(2I_x\right)^{\frac{j+k-1}{2}} \left(2I_y\right)^{\frac{l+m}{2}} e^{i\left[(1-j+k)\left(\psi_x+\psi_{x_0}\right)+(m-l)\left(\psi_y+\psi_{y_0}\right)\right]}. \end{aligned} \tag{2.30}$$

At this point, Eq. 2.30 is starting to look as a useful Fourier expansion. Ultimately, the data that can be extracted from a circular accelerator will come from a diagnostic device triggered every turn, i.e., turn-by-turn data. For that reason, it will be useful to rewrite Eq. 2.30 in terms of the N number of turns of particles in the accelerator. The expression relating the phase advances to the turn number reads:

$$\psi_u = 2\pi Q_u N, \tag{2.31}$$

where $2\pi Q_u$ is the respective phase advance over one turn of the accelerator, i.e. the tune of the circular accelerator.

Therefore, the resonance basis can be built by getting the quantity $h_u^{\pm} = \hat{u} \pm \hat{p}_u$ in terms of the number of turns N and using Eq. 2.31. Specifically, for h_x^- this reads:

$$\begin{aligned} h_x^-(N) = &\sqrt{2I_x} e^{i\left(2\pi Q_x N + \psi_{x_0}\right)} \\ &- 2i \sum_{jklm} j f_{jklm} \left(2I_x\right)^{\frac{j+k-1}{2}} \left(2I_y\right)^{\frac{l+m}{2}} e^{i\left[(1-j+k)\left(2\pi Q_x N+\psi_{x_0}\right)+(m-l)\left(2\pi Q_y N+\psi_{y_0}\right)\right]}, \end{aligned} \tag{2.32}$$

where Q_x and Q_y are the horizontal and vertical uncoupled tune. Note that this analysis can be easily extended to calculate the other elements in $\vec{h}$. These calculations are left as an exercise for the reader.

2.6 Space Charge Tune Shift

Up to this point, everything has been explained in terms of single-particle dynamics. Nevertheless, particles interact with each other through the Coulomb force. As mentioned in Sec. 2.4, the Coulomb force will act as a detuning force on each individual particle.

CHAPTER 3

THE FNAL RECYCLER RING

The Fermilab Recycler Ring (RR) is one of the circular accelerators located in the Fermilab Accelerator Complex. It was originally designed to store and accumulate antiprotons that remained from a Tevatron event [13]. The recycling of antiprotons was deemed ineffective and was never operationally implemented [14]. Since 2011, the RR has been repurposed to act as a pre-injector to the Main Injector (MI) by storing and accumulating protons [15]. It is worth pointing out, that the MI and the RR share the same tunnel, which has a circumference of 3.319 km (2.062 mi).

The MI/RR complex is fed protons by the Proton Source, which by itself consists of the Pre-Accelerator, the Linear Accelerator (Linac), and the Booster. The Pre-Accelerator systems provide H^- ions to the Linac, where they are accelerated to an energy of 400 MeV. After this, the beam is injected into the Booster Ring. The Booster is a rapid-cycling synchrotron operating at a 15 Hz repetition rate. During this injection process, the H^- beam passes through a carbon stripping foil, and it incorporates to the circulating proton beam. The Booster ramps the energy up from 400 MeV to 8 GeV. This 8 GeV proton beam can either go to the Booster Neutrino Experiments or get injected into the Recycler Ring. Once in RR the beam has two possible destinations: 1) high energy neutrino experiments through MI or 2) Muon Campus. For the latter, proton beam gets rebunched from 53 MHz to 2.5 MHz and transported to Muon Campus. For high energy neutrino experiments, the proton beam gets slip-stacked, hence doubling the intensity that gets injected into Main Injector. Once in MI, the beam is accelerated to 120 GeV and sent to the NuMI (Neutrinos at the Main Injector) beam facility [14–16]. A description of the accelerator complex is shown in figure 3.1, including the experimental beamlines which feed neutrino, muon and fixed target experiments.

The work done for this thesis focuses on the Recycler Ring. The following chapter starts by giving a general description for the operation and physics of the Recycler Ring. The next sections introduce and motivate the compensation of third order resonances for high intensity operation.

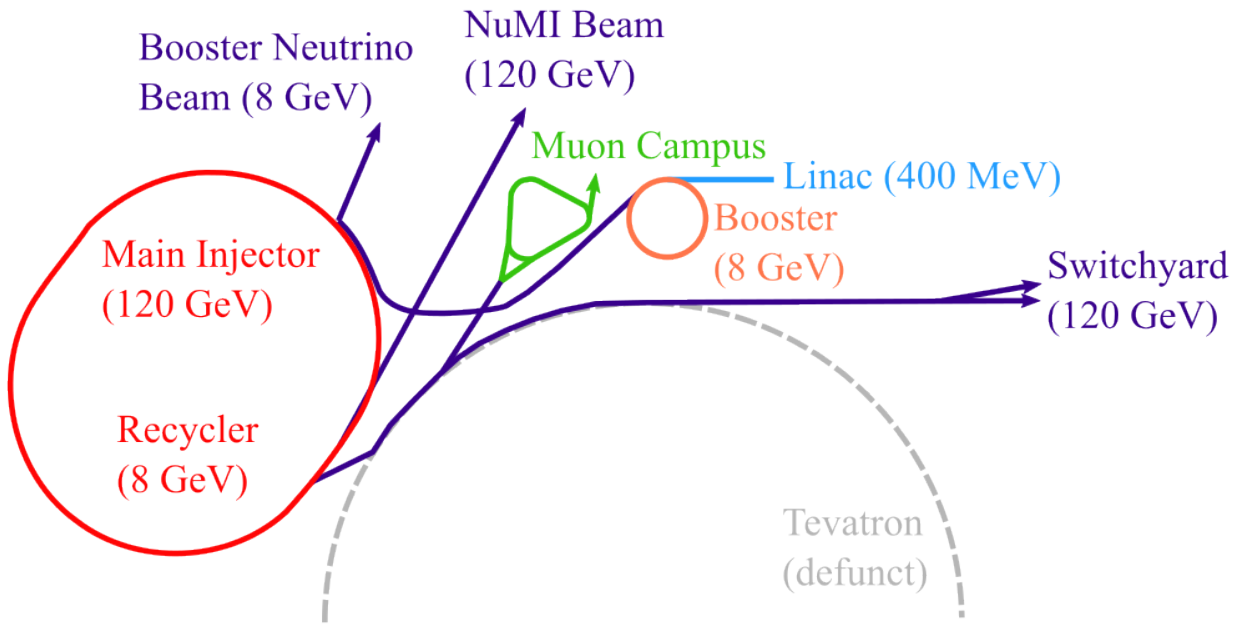

Figure 3.1 The past (Tevatron), present and future (PIP-II and LBNF) of the FNAL Accelerator Complex, taken from [3].

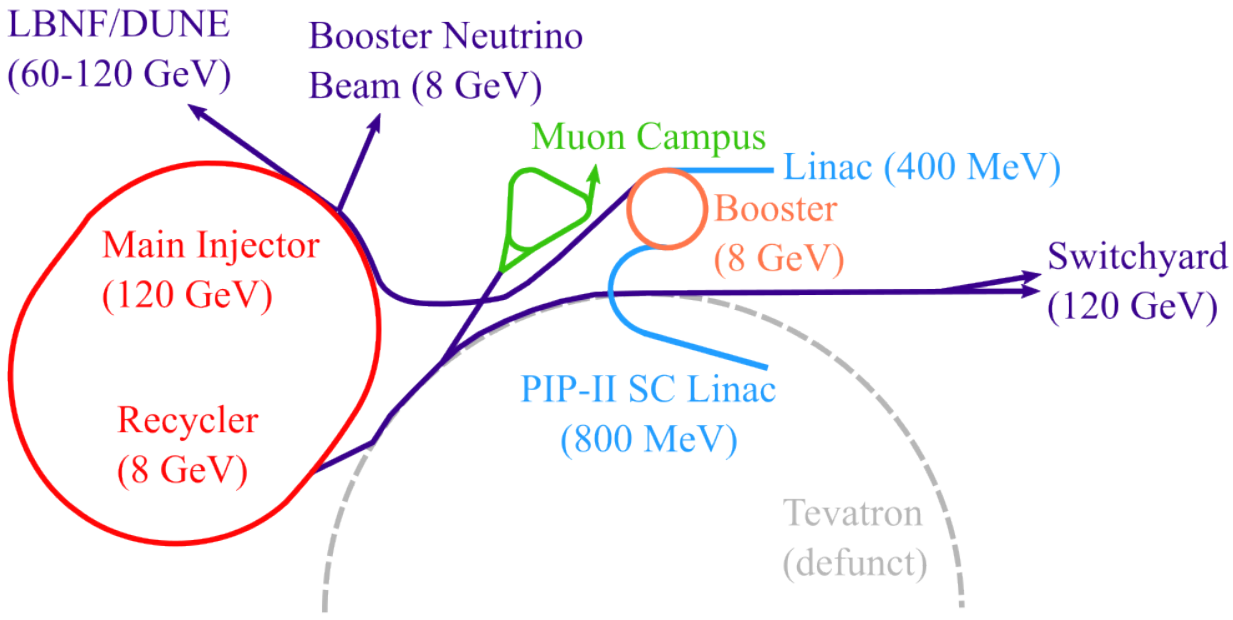

Figure 3.2 The past (Tevatron), present and future (PIP-II and LBNF) of the FNAL Accelerator Complex, taken from [3].

3.1 General Specifications

The RR is a permanent magnet storage ring operating at a fixed momentum of 8.835 Gev/c. [17] [18]

Table 3.1 Typical Recycler Ring properties for beam sent to NuMI

Parameter	**Value**	**Unit**
Circumference	3319	m
Momentum	8.835	GeV/c
RF Frequency	52.8	MHz
RF Voltage	80	kV
Harmonic Number	588	
Synchrotron Tune	0.0028	
Slip Factor	-8.6×10^{-3}	
Superperiodicity	2	
Horizontal Tune	25.43	
Vertical Tune	24.445	
Horizontal Chromaticity	-6	
Vertical Chromaticity	-7	
95% Normalized Emittance	15	π mm mrad
95% Longitudinal Emittance	0.08	eV s
Intensity	5×10^{10}	ppb
	8×10^{10} (PIP-II)	ppb
MI Ramp Time	1.2	s
	1.133	s
	1.067	s
Booster Frequency	15	Hz
	20 (PIP-II)	Hz

3.2 Tune Diagram and Resonances

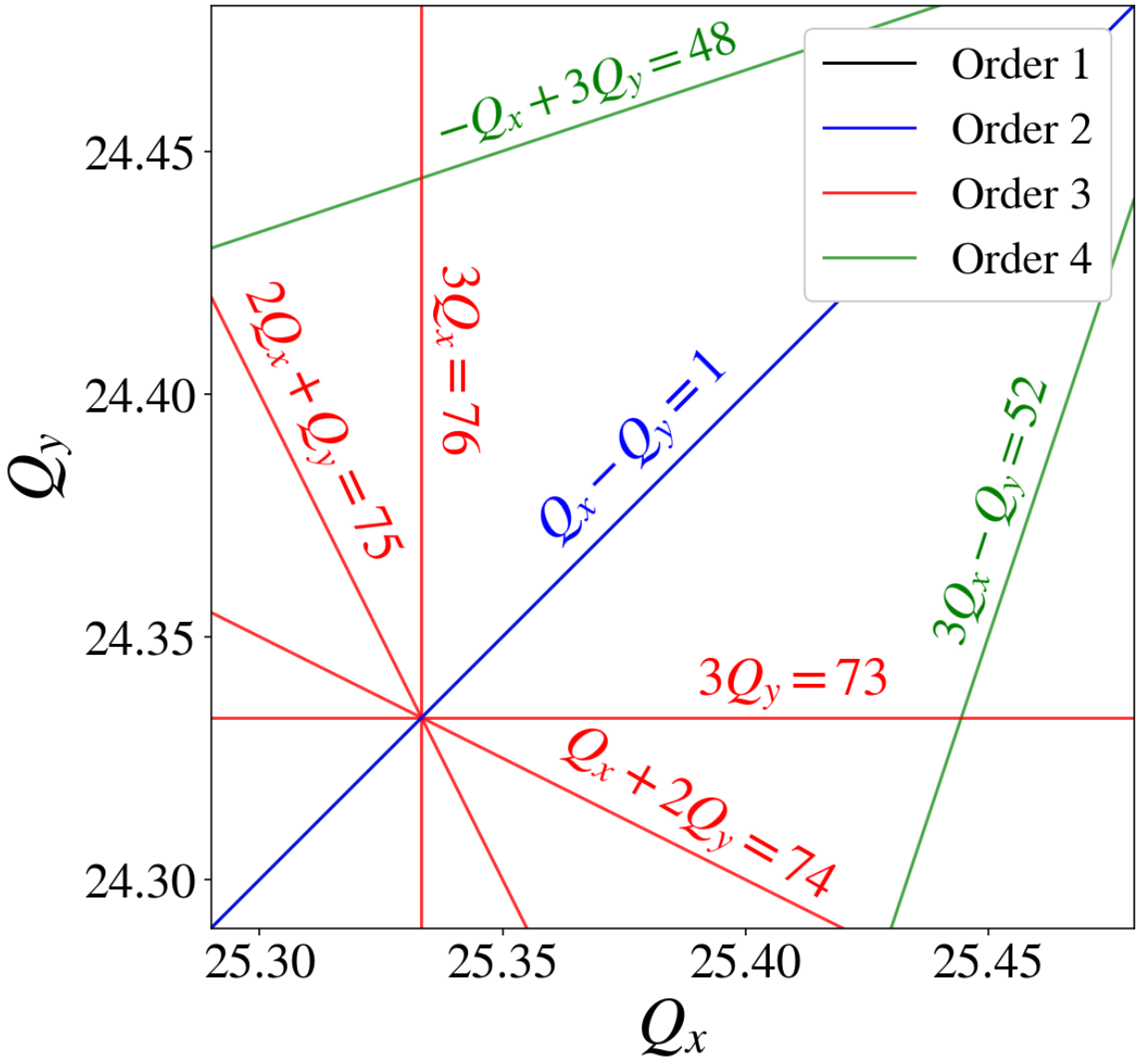

Figure 3.3 Portion of the tune diagram enclosing the operational tunes of the Recycler Ring.

3.3 High Intensity and Tune Footprint

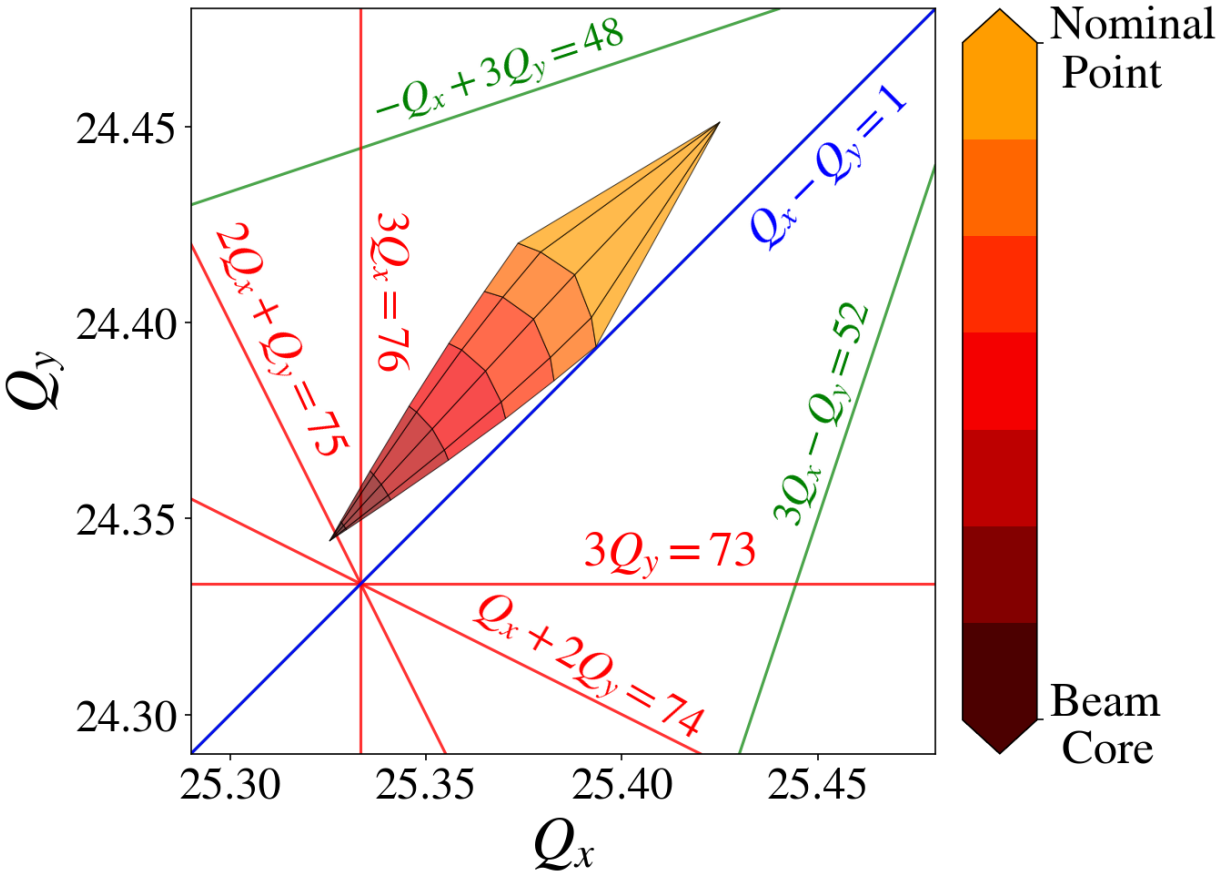

Figure 3.4 Approximate operational tune footprint at high intensities, i.e., 1e11 particles per bunch.

CHAPTER 4

COMPENSATION OF THIRD-ORDER RESONANCES AT LOW INTENSITIES

4.1 Global RDTs and Lattice Model

4.2 Measurement of Third Order RDTs

4.3 Compensation of RDTs

4.4 Optimization of Compensation Currents

4.5 Experimental Verification of Compensation

4.5.1 Dynamic Loss Map

4.5.2 Static Tune Scans

CHAPTER 5

RESONANCE COMPENSATION STUDIES AT THE CERN PROTON SYNCHROTRON BOOSTER

5.1 General specifications

5.2 Tune Diagram and Operation

5.3 Optimization Algorithms for Resonance Compensation

5.4 Experimental Verification of Compensation

CHAPTER 6

HIGH INTENSITY STUDIES

6.1 Global RDTs and Intensity-Dependent Effects

[19]

6.2 Space Charge Tune Shift

6.3 Measurement of Tune Shift

6.4 Static Tune Scans at Different Intensities

CHAPTER 7

CONCLUSIONS AND FUTURE WORK

[20] [21]

BIBLIOGRAPHY

[1] S Y Lee. *Accelerator Physics*. 3rd. WORLD SCIENTIFIC, 2011. DOI: 10.1142/8335. eprint: https://www.worldscientific.com/doi/pdf/10.1142/8335. URL: https://www.worldscientific.com/doi/abs/10.1142/8335.

[2] David Griffiths. "Historical Introduction to the Elementary Particles". In: *Introduction to Elementary Particles*. John Wiley and Sons, Ltd, 1987. Chap. 1, pp. 11–53. ISBN: 9783527618460. DOI: https://doi.org/10.1002/9783527618460.ch1. eprint: https://onlinelibrary.wiley.com/doi/pdf/10.1002/9783527618460.ch1. URL: https://onlinelibrary.wiley.com/doi/abs/10.1002/9783527618460.ch1.

[3] Étienne Forest. *Beam Dynamics: A New Attitude and Framework*. Vol. 8. The Physics and Technology of Particle and Photon Beams. Amsterdam, The Netherlands: Hardwood Academic / CRC Press, 1998. ISBN: 978-90-5702-574-7.

[4] S. Holmes et al. "Accelerator physics at the Tevatron Collider: Introduction". In: *Accelerator physics at the Tevatron Collider*. Ed. by Valery Lebedev and Vladimir Shiltsev. 2014, pp. 1–28. DOI: 10.1007/978-1-4939-0885-1_1.

[5] Lillian Hoddeson, Adrienne W. Kolb, and Catherine Westfall. *Fermilab: Physics, the Frontier, and Megascience*. University of Chicago Press, Dec. 2008. ISBN: 9780226346236. DOI: 10.7208/chicago/9780226346250.001.0001. URL: https://doi.org/10.7208/chicago/9780226346250.001.0001.

[6] Andrzej Wolski. *Beam Dynamics in High Energy Particle Accelerators*. 2nd. WORLD SCIENTIFIC, 2023. DOI: 10.1142/13333. eprint: https://www.worldscientific.com/doi/pdf/10.1142/13333. URL: https://www.worldscientific.com/doi/abs/10.1142/13333.

[7] T. Satogata. *Lecture Notes on Poisson Brackets and Lie Operators*. https://toddsatogata.net/2011-USPAS/lieAlgebras.pdf. Jan. 2008.

[8] P. Urschutz. "Measurement and Compensation of Betatron Resonances at the CERN PS Booster Synchrotron". PhD thesis. Vienna, Austria, 2004.

[9] R. Tomas Garcia. "Direct Measurement of Resonance Driving Terms in the Super Proton Synchrotron (SPS) of CERN using Beam Position Monitors". PhD thesis. Valencia, Spain, Jan. 2003.

[10] Rüdiger Achilles and Andrea Bonfiglioli. "The early proofs of the theorem of Campbell, Baker, Hausdorff, and Dynkin". In: *Archive for History of Exact Sciences* 66.3 (May 2012), pp. 295–358. DOI: 10.1007/s00407-012-0095-8. URL: https://doi.org/10.1007/s00407-012-0095-8.

[11] R Bartolini and F Schmidt. "Normal form via tracking or beam data". In: *Part. Accel.* 59 (1998), pp. 93–106. URL: https://cds.cern.ch/record/333077.

[12] Helmut Wiedemann. *Resonances*. Cham: Springer International Publishing, 2015, pp. 539–564. ISBN: 978-3-319-18317-6. DOI: 10.1007/978-3-319-18317-6_16. URL: https://doi.org/10.1007/978-3-319-18317-6_16.

[13] G. Jackson. *The Fermilab recycler ring technical design report. Revision 1.2*. Tech. rep. FNAL-TM-1991ON: DE97051388; BR: KAHEP. Fermilab, Nov. 1996. DOI: 10.2172/16029. URL: https://www.osti.gov/biblio/16029.

[14] S. Nagaitsev. *Fermilab Antiproton source, Recycler ring and Main Injector*. Tech. rep. FERMILAB-FN-0957-AD. Fermilab, Mar. 2013. DOI: 10.2172/1127965. URL: https://www.osti.gov/biblio/1127965.

[15] R. Ainsworth et al. "High intensity operation using proton stacking in the Fermilab Recycler to deliver 700 kW of 120 GeV proton beam". In: *Phys. Rev. Accel. Beams* 23 (12 Dec. 2020), p. 121002. DOI: 10.1103/PhysRevAccelBeams.23.121002. URL: https://link.aps.org/doi/10.1103/PhysRevAccelBeams.23.121002.

[16] P. Adamson et al. "The NuMI neutrino beam". In: *Nuclear Instruments and Methods in Physics Research Section A: Accelerators, Spectrometers, Detectors and Associated Equipment* 806 (2016), pp. 279–306. ISSN: 0168-9002. DOI: https://doi.org/10.1016/j.nima.2015.08.063. URL: https://www.sciencedirect.com/science/article/pii/S016890021501027X.

[17] M. Ball et al. *The PIP-II Conceptual Design Report*. Tech. rep. FERMILAB-TM-2649-AD-APC1516858. Fermilab, Mar. 2017. DOI: 10.2172/1346823. URL: https://www.osti.gov/biblio/1346823.

[18] R. Ainsworth et al. "High intensity space charge effects on slip stacked beam in the Fermilab Recycler". In: *Phys. Rev. Accel. Beams* 22 (2 Feb. 2019), p. 020404. DOI: 10.1103/PhysRevAccelBeams.22.020404. URL: https://link.aps.org/doi/10.1103/PhysRevAccelBeams.22.020404.

[19] N. Chelidze, R. Ainsworth, and K.J. Hazelwood. "The Effect of the Main Injector Ramp on the Recycler". In: *Proc. 5th Int. Particle Accel. Conf. (NAPAC'22)* (Albuquerque, NM, USA). International Particle Accelerator Conference 5. JACoW Publishing, Geneva, Switzerland, Oct. 2022, MOPA19, pp. 90–92. ISBN: 978-3-95450-232-5. DOI: 10.18429/JACoW-NAPAC2022-MOPA19. URL: https://jacow.org/napac2022/papers/mopa19.pdf.

[20] C.E. Gonzalez-Ortiz, R. Ainsworth, and P.N. Ostroumov. "Third-Order Resonance Compensation at the FNAL Recycler Ring". In: *Proc. IPAC'22* (Bangkok, Thailand). International Particle Accelerator Conference 13. JACoW Publishing, Geneva, Switzer-

land, July 2022, MOPOST050, pp. 195–198. ISBN: 978-3-95450-227-1. DOI: 10.18429/JACoW-IPAC2022-MOPOST050. URL: https://jacow.org/ipac2022/papers/mopost050.pdf.

[21] C.E. Gonzalez-Ortiz, R. Ainsworth, and P.N. Ostroumov. "Simultaneous Compensation of Third-Order Resonances at the FNAL Recycler Ring". In: *Proc. IPAC'23* (Venezia). IPAC'23 - 14th International Particle Accelerator Conference 14. JACoW Publishing, Geneva, Switzerland, May 2023, pp. 3328–3331. ISBN: 978-3-95450-231-8. DOI: doi:10.18429/jacow-ipac2023-wepl112. URL: https://www.ipac23.org/preproc/pdf/WEPL112.pdf.

APPENDIX

YOUR APPENDIX